Desalination and Water Treatment
www.deswater.com
doi: 10.5004/dwt.2020.26185

202 (2020) 355–363
October

Enhanced photocatalytic ozonation of 2,4-dichlorophenoxyacetic acid using CoP cocatalyst decorated on g-C_3N_4 under visible light irradiation

Zhuo Liu[a], Changyu Lu[b,c,d,*], Qicai Mo[b], Qiaozhi Yan[b], Jinlin Li[d], Weisheng Guan[d]

[a]*Experimental Practising Teaching Center, Hebei GEO University, Shijiazhuang 050031, China, email: 12848197@qq.com (Z. Liu)*
[b]*School of Water Resources and Environment, Hebei Province Key Laboratory of Sustained Utilization and Development of Water Resources, Hebei Province Collaborative Innovation Center for Sustainable Utilization of Water Resources and Optimization of Industrial Structure, Hebei GEO University, Shijiazhuang 050031, China, Tel. +86-29-82334561; Fax: +86-29-82334566; emails: pzpzlxl@163.com (C.Y. Lu), 1296021022@qq.com (Q.C. Mo), yanqiaozhi123@126.com (Q.Z. Yan)*
[c]*School of Geology and Environment, Xi'an University of Science and Technology, Xi'an 710064, Shaanxi, China*
[d]*School of Environmental Science and Engineering, Chang'an University, Xi'an 710064, China, emails: cstsjz@163.com (J. Li), guanweisheng@263.net (W.S. Guan)*

Received 26 January 2020; Accepted 29 May 2020

ABSTRACT

Novel noble-metal-free CoP/g-C_3N_4 composite photocatalysts were synthesized using a solid-state-synthesis approach. 2,4-dichlorophenoxyacetic acid was used as a target pollutant to evaluate photocatalytic and photocatalytic ozonation performance of the as-prepared photocatalysts. Profiting from the efficient charge separation of the photogenerated carriers, with the addition of CoP as co-catalyst and the efficient scavenging of the photoinduced electrons by O_3, the composite of 0.5% CoP/g-C_3N_4 exhibited the highest photocatalytic ozonation performance (96.4%, 60 min, 30 mL/min O_3), which is about 3.77 and 2.96 times higher than that of single photocatalytic and ozonation, respectively. The synergy factor between photocatalysis and ozonation is 3.53, which shows the increased synergy rate between the photocatalytic and ozone oxidation.

Keywords: CoP/g-C_3N_4; Composite materials; Photocatalytic ozonation; 2,4-dichlorophenoxyacetic acid

1. Introduction

2,4-dichlorophenoxyacetic acid (2,4-D) is a well-known phenoxy herbicide and widely used for controlling broad-leaf weeds [1,2]. Due to its potential carcinogenic and mutagenic effect, it not only contaminates the soil and water body but also can damage the ecological equilibrium of the environment, affecting even human health [3,4]. Therefore, the removal of 2,4-D has become an important environmental issue and has been intensively researched. Photocatalysis is an advanced oxidation process [5,6], which has received much attention in recent years due to its photocatalytic oxidation reaction to decompose organic matter into carbon dioxide and water, with light as energy [7–9].

TiO_2 [10] and ZnO [11] are the most promising semiconductor photocatalytic materials due to the advantages of high stability, nontoxicity and low-cost. Nevertheless, the wide bandgap limits their range of visible-light absorption seriously ($\lambda \leq 387$ nm) [12,13]. g-C_3N_4 is a kind of non-metallic organic polymer photocatalytic semiconductor ($E_g \approx 2.7$ eV) and is regarded as a new and efficient way to solve current environmental pollution with its advantages of low synthesis costs, environmental friendliness, simple operation, and high thermal and chemical stability [14,15]. However, its photocatalytic activity is confined by the relatively poor quantum yield resulting from the low charge separation rate of photogenerated electron-hole pairs

* Corresponding author.

[16,17]. Over the years, various efforts have been made to enhance the photocatalytic activity of this material, such as doping with metal/non-metal ions [18], deposition of transition metals [19] and noble metal [20], synthesis of composites [21], the formation of heterojunctions [22] and modification with co-catalysts [23]. Among these methods, the effort of modification with metal phosphides co-catalysts are similar to the deposition of transition metals and noble metal, both of them can improve the separation efficiency of photogenerated carriers on the surface of photocatalyst, resulting in highly effective interfacial charge transfer [24]. Qi et al. [25] reported that, after Ag loading, the Ag/g-C_3N_4 composites expand the visible light response and show an enhanced photocatalytic activity on RhB decomposition, which is 10 times of the rate of pure C_3N_4. However, due to the expensive and scarce of noble metals, it limits the large-scale application in reality. Therefore, the development of highly active and non-noble-metal cocatalysts are desirable for industrial catalysis. Theoretically, modification with CoP co-catalysts can be an efficient pathway for improving the photocatalytic activity of the main catalyst due to its excellent activity, stability and electrical conductivity [26]. To the best knowledge of the authors, some references on CoP/g-C_3N_4 binary catalyst have been already reported [27–29], but these investigations are mainly focusing on photocatalytic hydrogen production, the photocatalytic degradation of emerging pollutants has not been reported, yet. Moreover, it can be an efficient scavenger for the photoinduced electrons, which could significantly promote the charge separation efficiency.

In this work, CoP nanoparticles were selected as a non-precious metal cocatalyst for g-C_3N_4, and CoP/g-C_3N_4 (CoP/CN) composite catalysts were successfully prepared and used for enhanced photocatalytic ozonation of 2,4-D pollutants under visible light irradiation.

2. Material and methods

2.1. Material

All chemicals in this study were of analytical grade without any further purification. Annealing urea (AR, CH_4N_2O), sodium hydroxide (AR, NaOH), cobaltous nitrate (AR, $Co(NO_3)_2{\cdot}6H_2O$), sodium citrate (AR, $Na_3C_6H_5O_7{\cdot}2H_2O$), sodium hydrogen phosphate (AR, $NaH_2PO_4{\cdot}2H_2O$), ethanol (AR, C_2H_5OH) were purchased from Sinopharm Chemical Reagent Co., Ltd., (China). 2,4-D was purchased from Shanghai Zhanyun Chemical Co., Ltd., (China).

2.2. Preparation of catalysts

The g-C_3N_4 was synthesized by annealing urea in a muffle furnace [30]. 10 g urea powder was placed in a covered alumina crucible, heated to 550°C in a muffle furnace at a speed of 0.5°C/min, and kept at this temperature for 3 h. The obtained products were ground into powders after cooling down to room temperature. Next, the products obtained as above were placed in an open ceramic container and heated to 500°C with a ramp rate of 2°C/min and maintained at this temperature for 2 h. A light yellow powder of g-C_3N_4 was finally obtained.

100 mL 0.5 M NaOH solution was added into a 100 mL solution containing 200 mg of $Co(NO_3)_2$ and 50 mg of sodium citrate. After centrifugation, the precipitate was separated and dried in a vacuum oven to obtain the $Co(OH)_2$ precursor. Then, 0.05 g of $Co(OH)_2$ and 0.25 g of NaH_2PO_2 were added into agate mortar and completely grounded. In the next step, the mixture was heated at 300°C for 2 h at a heating rate of 1°C/min (under inert/argon atmosphere). Finally, the resulting black solid was collected by centrifugation and washed with distilled water and ethanol several times, thus obtained the CoP powder. For CoP/g-C_3N_4, the 0.5 wt.% CoP/g-C_3N_4 composite sample was used as an example. 200 mg g-C_3N_4 were dispersed in 40 mL ethanol, stirred and dispersed with ultrasonication. 1 mg CoP was added into the above solution and stirred until it was dried, and obtaining the CoP/g-C_3N_4 composites. CoP/g-C_3N_4 composites with different ratios (0.1, 0.5, 1, 3, and 7 wt.%) were prepared under similar conditions and labelled 0.1%-CoP/CN, 0.5%-CoP/CN, 1%-CoP/CN, 3%-CoP/CN, and 7%-CoP/CN.

2.3. Characterization

The crystalline form and crystallinity of the obtained sample were analyzed by powder X-ray diffraction (XRD, D8 Discover, Bruker, Germany) technique equipped with Cu-Kα radiation (λ = 0.154178 nm). The microscopic morphology and the elements of the synthesized powder samples were analyzed using an S-4800 scanning electron microscopy (SEM) instrument and an energy-dispersive X-ray spectrometer (EDS) (Hitachi, Japan). The UV-Vis absorption spectra were determined by UV-Vis spectrophotometer (UV2550, Shimadzu, Japan) with barium sulfate as the reference. The photoluminescence study was recorded on the Fluorolog-TCSPC luminescence spectrometer (Japan). The electrochemical analysis was conducted on a CHI 760C workstation. The transient photocurrent response analysis was conducted in 0.5 M Na_2SO_4 electrolyte under 300 W Xe lamp irradiation. Electrochemical impedance spectroscopy (EIS) was recorded by using an alternating voltage of 5 mV amplitude in the frequency range of 10^5 Hz to 10^{-2} Hz with the open-circuit voltage in 0.5 M Na_2SO_4.

2.4. Evaluation of photocatalytic activity

The photocatalytic properties of the samples were evaluated by degrading 2,4-D under irradiation with a 300 W Xenon lamp. Briefly, 40 mg of the photocatalyst was suspended in 50 mL of 2,4-D solution with an initial concentration of 20 mg/L. The mixture was placed in a light reaction chamber and magnetically stirred in the dark for 30 min to reach adsorption–desorption equilibrium. Subsequently, visible light (300 W, Xenon lamp) was obtained by using cut off filters to remove light of λ < 420 nm, a mixture of ozone and oxygen (14.2 mg/L ozone concentration) was fed to the reactor at a flow rate of 30 mL/min. The lamp-to-sample distance is 8 cm and the pH of the 2,4-D solution is 6.5. O_3 comes from the Ozonator (FL-803A, Shenzhen Feili Electrical Technology Co., Ltd., China). The solution was magnetically stirred continuously, and a sample was collected every 10 min. After centrifugation, 3 ml supernatant was collected and analyzed by a UV-Vis spectrophotometer

at a maximum wavelength of 283 nm to determine the concentration of the aqueous solution. The degradation rate was calculated by the following formula:

$$\text{Degradation}\ (\%) = \left[\left(1-\frac{A_i}{A_0}\right)\right]\times 100\%. \quad (1)$$

where A_0 is the absorbance of the initial solution and A_i is the absorbance of the solution after the reaction.

3. Results and discussion

3.1. XRD and UV-Vis

XRD patterns were taken to elucidate the structural composition of the obtained materials and shown in Fig. 1a. For pure g-C_3N_4, two characteristic diffraction peaks can be observed at 13.1° and 27.4°, which are corresponding to the (100) and (002) crystal facets and attributing to in-plane structural packing motif and interlayer stacking of aromatic segments, respectively [31]. All the diffraction peaks are attributed to the orthorhombic CoP [32]. For CoP/CN, the peaks of CoP are clearly observed just in the case of 7%-CoP/CN, due to the low content of CoP and the sensitivity of the method. Fig. 1b shows the UV-Vis spectra of as-synthesized samples. It reveals that all the samples exhibit intensive light absorption in the visible-light range. The light absorption of g-C_3N_4 can be extended from the ultraviolet region to a visible region with a band edge of about 450 nm. For CoP, it has a particularly pronounced light absorption in the 200–800 nm wavelength region. It should be noted that, after the combination of CoP and g-C_3N_4, the composite has a slight redshift, and the absorption intensity is enhanced in the visible-light region, which indicates that the introduction of CoP slightly improves the light absorption [33].

3.2. Scanning electron microscopy

The morphology of as-synthesized samples was investigated by SEM. From Fig. 2a, it can be observed that the CoP is composed of nanoparticles with an average size of 30–50 nm and shows an agglomerated morphology. In Fig. 2b it can be observed that the g-C_3N_4 is formed by pleats and stacked floc structures. In Fig. 2c, when g-C_3N_4 is combined with 0.5% of CoP, the CoP particles are deposited on the surface of g-C_3N_4. Moreover, EDS measurements were employed to test the distribution of CoP particles. The results showed that the only elements are Co and P which can be detected in the pure CoP, and the atomic ratio of elements is nearly 1:1, which further confirms that the CoP has been successfully prepared.

3.3. Transmission electron microscopy

The morphologies of 0.5%-CoP/CN composite were observed by transmission electron microscopy (TEM) and high-resolution transmission electron microscopy (HRTEM). As exhibited in Fig. 3a, TiO_2 nanoparticles are distributed on the surface of g-C_3N_4. Furthermore, the HRTEM image in Fig. 3b displays the interplanar spacing of CoP and C_3N_4 are 0.28 and 0.33 nm, corresponding to the (101) planes and (002) planes, respectively. Therefore, it can be proved that an integrated heterostructure can be formed between CoP and C_3N_4 [34].

3.4. Catalytic performance

The photocatalytic ozonation activity of CoP/CN composites was evaluated by degrading 2,4-D under visible-light irradiation (PO/Vis). In Fig. 4a, pure CoP and g-C_3N_4 exhibited negligible photocatalytic performance toward the pollutant, obtaining degradation rates about 5% and 4.77% after 1 h visible-light irradiation (LFO/O_2/Vis), respectively. When adding 0.5 wt.% CoP, the composite shows the highest photocatalytic degradation efficiency of 17.1%. On the other hand, with the increase of CoP content in the composites, the photocatalytic activity decreases gradually. Generally, it can be concluded that the photocatalytic degradation efficiencies are very low, not giving the desired degradation yields to be able to consider the applicability of the composites in this form in the practical water treatment. In Fig. 4b, the results obtained are shown when ozone is introduced into the photocatalytic system, giving obviously increased degradation rates for

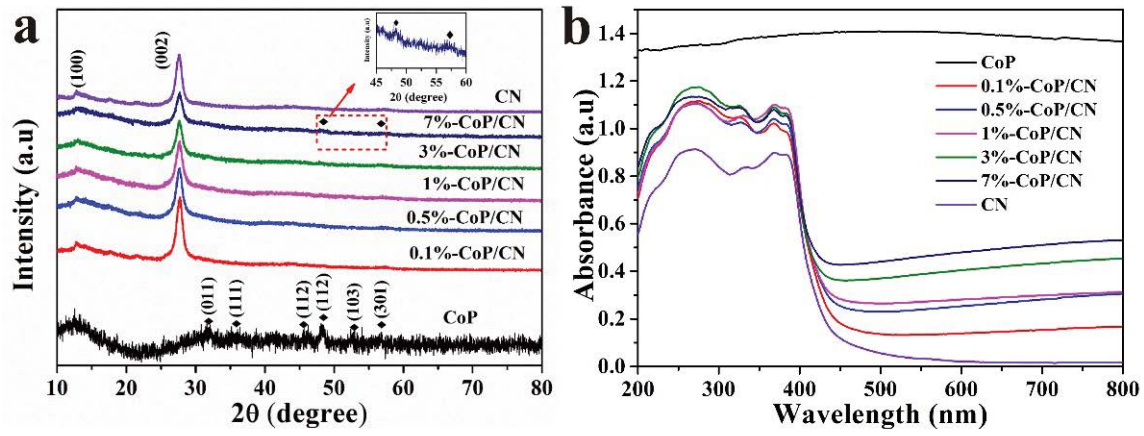

Fig. 1. XRD patterns (a) and UV-Vis spectra (b) of the as-synthesized samples.

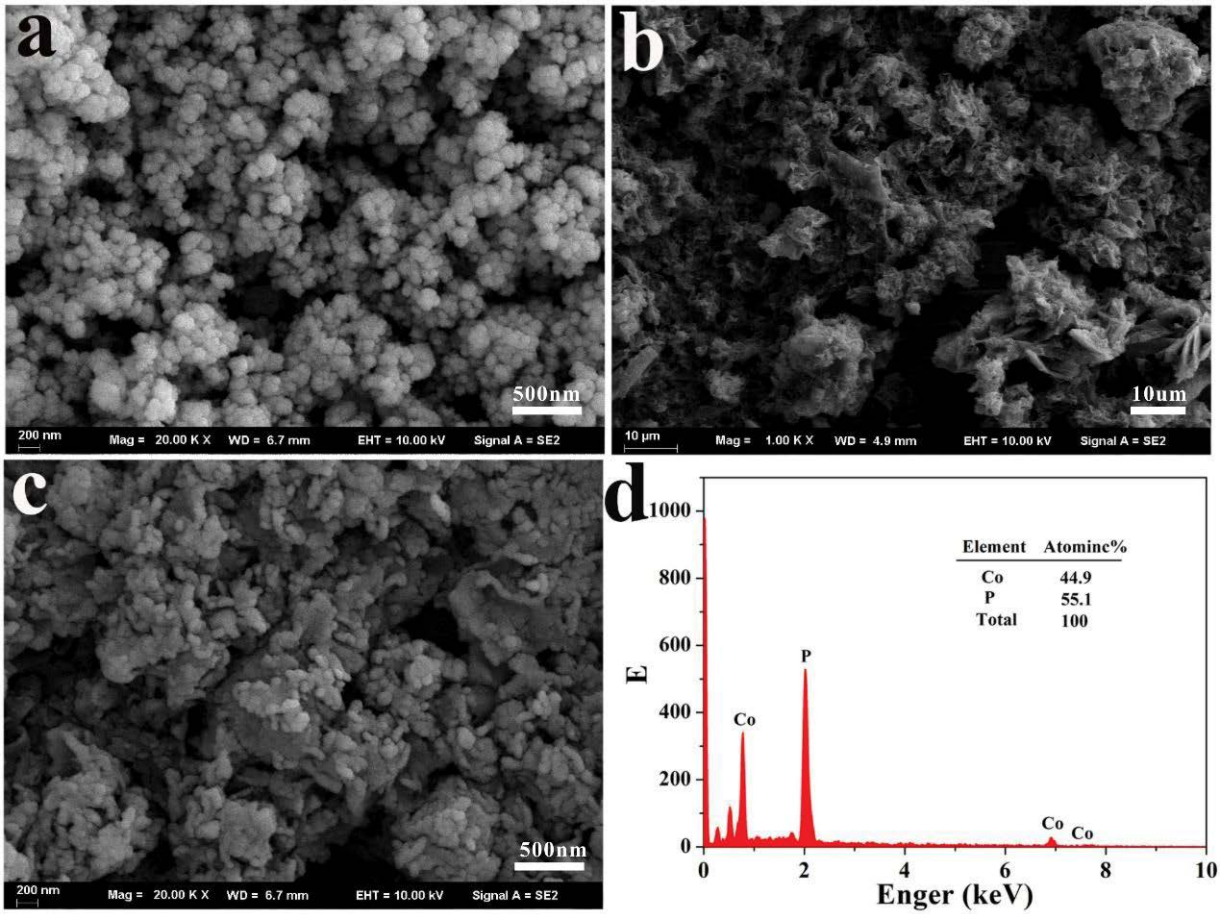

Fig. 2. SEM images of (a) CoP, (b) g-C_3N_4, (c) 0.5%-CoP/CN, and (d) EDS of CoP.

the 2,4-D. The 0.5%-CoP/CN composite maintained its "winner place", showing the highest ozone-enhanced photocatalytic activity of 96.4%. Meanwhile, to better understand the synergy between photocatalysis and ozonation in CoP/CN photocatalytic ozonation system, the ozonation degradation and first-order kinetics of 2,4-D degradation are also performed. As shown in Fig. 4c, different kinds of catalysts had little influence on the ozonation, and the degrading rate of each sample is about 60%, indicating the degradation performance of ozonation alone. In Fig. 4d, the pseudo-first-order rate constants for ozone-enhanced photocatalysis (Vis/0.5%-CoP/CN/O_3), ozonation (Vis/O_3) and photocatalysis (Vis/0.5%-CoP/CN) is 0.0342, 0.0089 and 0.0008 min^{-1}, respectively. The synergistic factors in photocatalytic ozonation of 2,4-D can be determined by the following equation [35]:

$$\text{Synergistic Factor}(\text{SF}) = \frac{K_{app}\text{photocatalytic ozonation}}{K_{app}\text{photolytic ozonation} + K_{app}\text{photocatalytic oxidation}} = \frac{0.0342}{0.0089 + 0.0008} = 3.53 > 1 \quad (2)$$

The synergistic factor is 3.53, indicating that the two degrading technologies have synergistic effects rather than the simple accumulation of oxidation. Furthermore, by comparison, with other previously reported photocatalytic ozonation photocatalysts (Table S1), it is found that CoP/CN composite exhibits better photocatalytic degradation performance, which proves that the CoP/CN composite possesses the broad prospect in the field of wastewater treatment.

It is well-known that the stability of photocatalyst is key to determine whether it can be put into practical application. Thus, the 0.5%-CoP/CN sample was further chosen as the photocatalyst for the cycling experiment. As shown in Fig. 5a, the degradation rate was still over 90% after five cycling runs, indicating the extraordinary stability and reusability of the 0.5%-CoP/CN sample. Total organic carbon (TOC) removal is an effective method to further demonstrate the mineralisation of organic pollutants. In Fig. 5b, the removal rates of TOC of pure CoP, g-C_3N_4, 0.1%-CoP/CN, 0.5%-CoP/CN, 1%-CoP/CN, 3%-CoP/CN, and 7%-CoP/CN were 46.9%, 60.3%, 80.2%, 88.2%, 79.9%, 78.2%, and 78.9%, respectively. TOC contents decreased in the same order as that of the photocatalytic degradation curves. However, the removal rates of TOC were lower

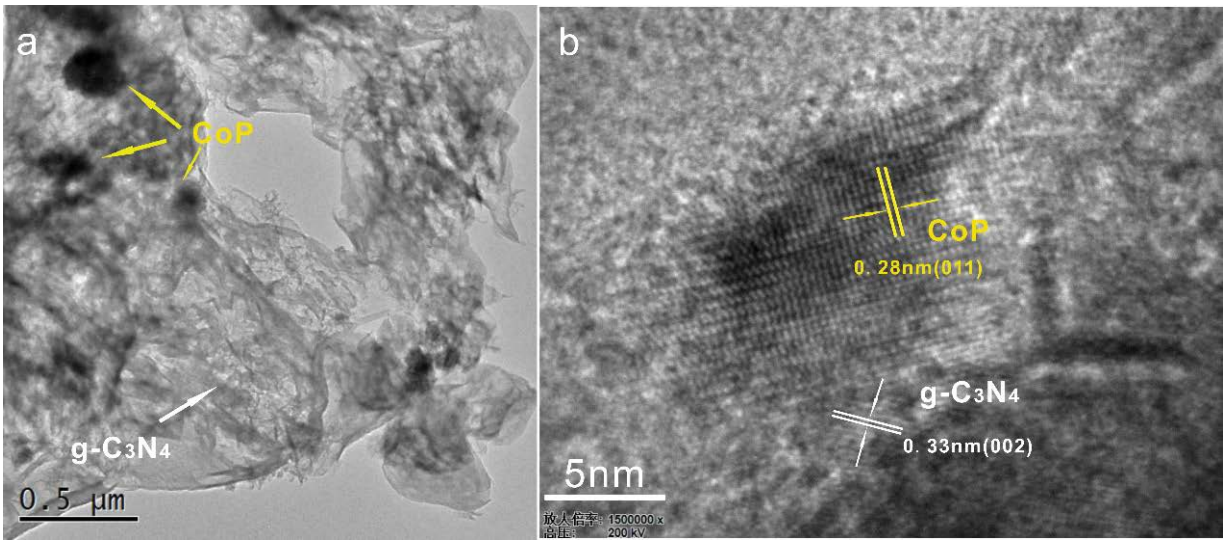

Fig. 3. TEM (a) and (b) HRTEM images of 0.5%-CoP/CN samples.

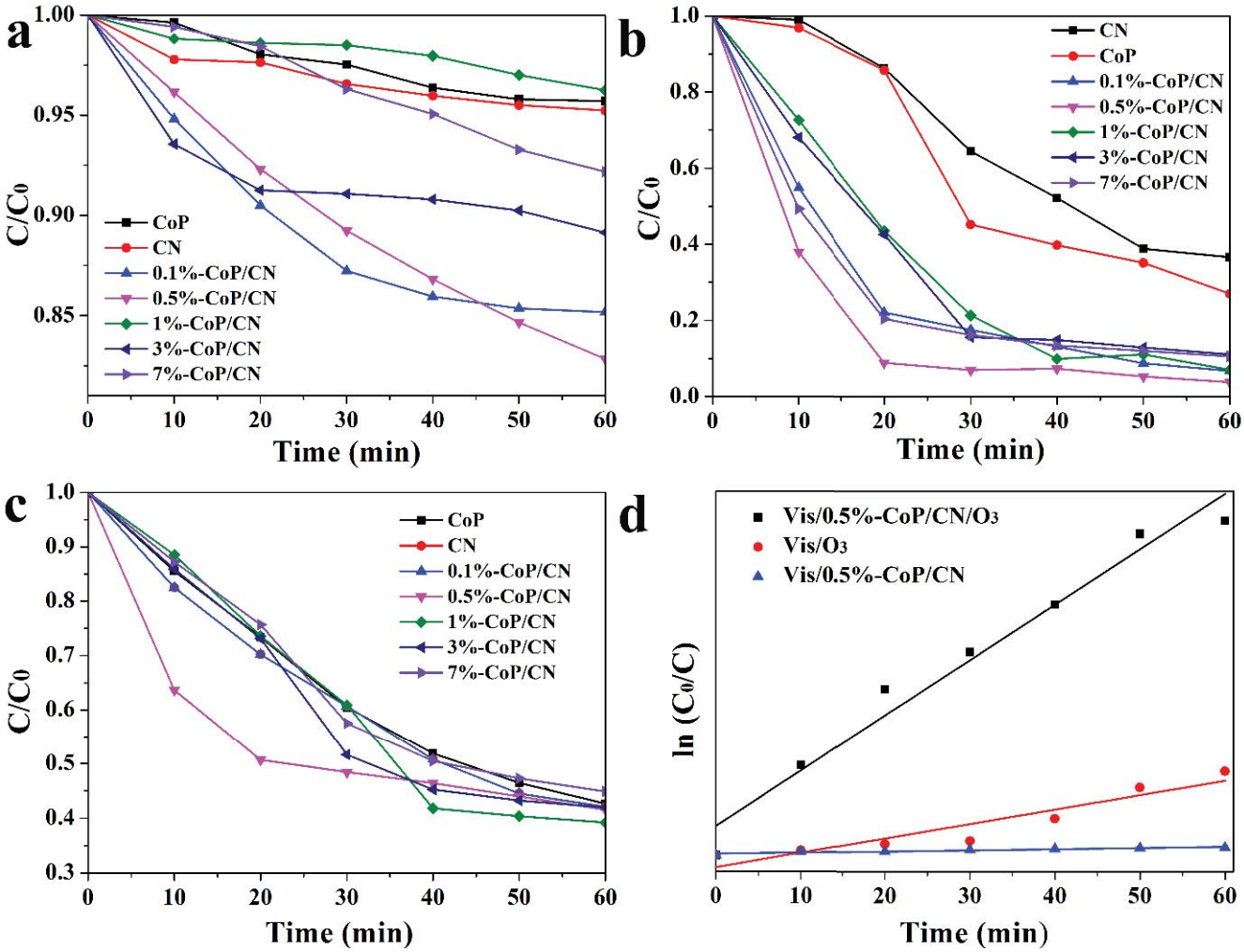

Fig. 4. (a) Photocatalytic, (b) photocatalytic ozonation degradation of 2,4-D over as-synthesized photocatalysts under visible-light irradiation, (c) ozonation degradation of 2,4-D over as-prepared samples under visible light, and (d) first-order kinetic of 2,4-D degradation over 0.5%-CoP/CN by different processes.

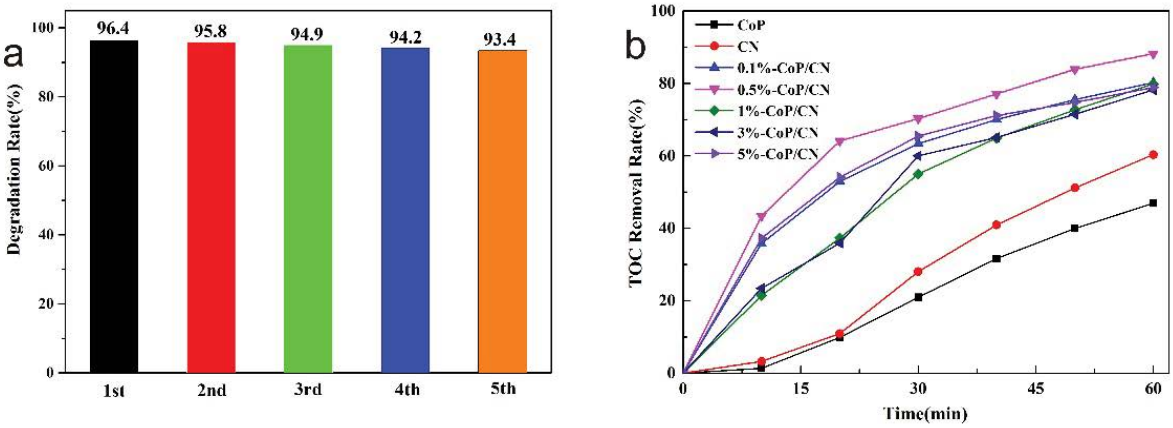

Fig. 5. (a) Cycling runs for the photocatalytic oxidation degradation of 2,4-D in the presence of 0.5%-CoP/CN and (b) TOC removal of 2,4-D on as-synthesized photocatalysts.

than that of the degradation. This result was reasonable due to the degradation data were detected after centrifugation. Moreover, widely environmental applications, such as the mineralization, would be implemented by CoP/CN, since the reduced TOC contents suggested.

3.5. Photocurrent response and EIS

Photocurrent response is used to further demonstrate the efficiency of the charge transfer in CoP/CN composites. According to Fig. 6a, it was evident that both pure g-C_3N_4 and CoP show lower photocurrent intensities due to the high recombination rate of photo-generated carriers. Notably, the photocurrent density increases after the formation of CoP/g-C_3N_4 composites. It is also proved that the 0.5%-CoP/CN composite has the fastest transfer rate of photo-generated electrons and leads to more efficient separation of electron-hole pairs. EIS was also involved in exploring the charge-transfer impedance and photogenerated electron-hole pair transmission. 0.5%-CoP/CN composite had the smallest radian, which further proves that CoP/CN composites revealed accelerated interfacial charge migration rate, resulting in increased efficiency of the separation of photogenerated carriers.

3.6. Active species capturing experiment

To investigate the photocatalytic mechanism of CoP/CN, active species capturing experiment in the ozone-enhanced photocatalysis degradation is performed and displayed in Fig. 7. EDTA-2Na, $CHCl_3$, and tBA are used to capture h^+, $^{\bullet}O_2^-$, and $^{\bullet}OH$, respectively [36]. When adding $CHCl_3$ the degrading rate remains at about 80%, which indicates that $^{\bullet}O_2^-$ is not the main active species. After adding EDTA-2Na and tBA, the photocatalytic activity is significantly inhibited and the degrading rate is 30.5% and 39.5%, respectively, which indicating that h^+ and $^{\bullet}OH$ are the main active species in the system. Under a N_2 atmosphere, the photocatalytic activity is significantly inhibited and the degrading rate is 32.3%, it shows that ozone played an important role in the degradation activity. The results indicate that h^+ and $^{\bullet}OH$ are the main active species.

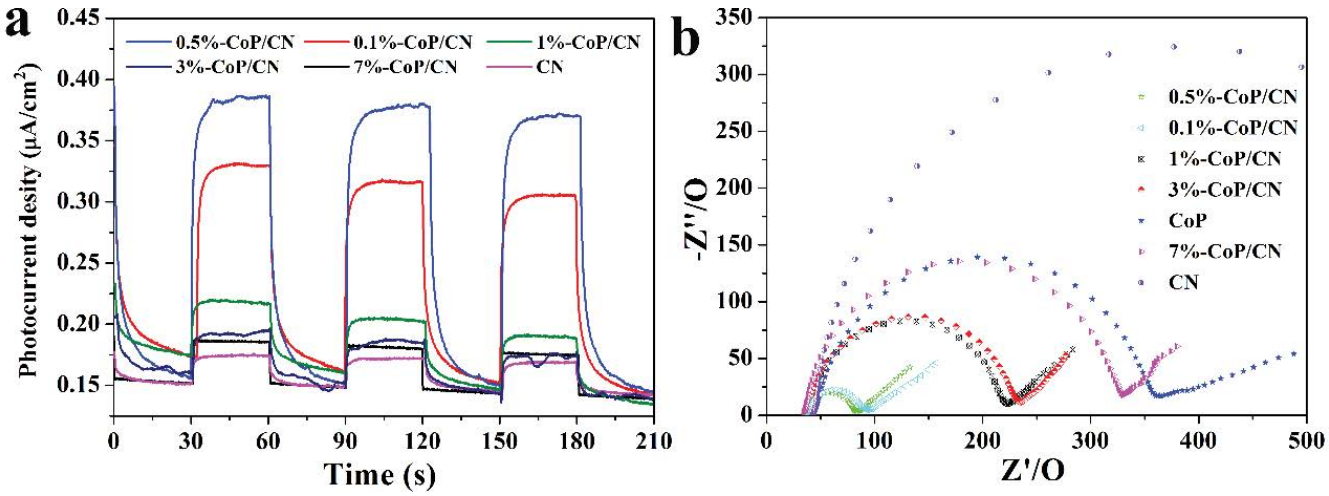

Fig. 6. (a) Photocurrent responses and (b) EIS Nyquist plot of as-synthesized photocatalysts.

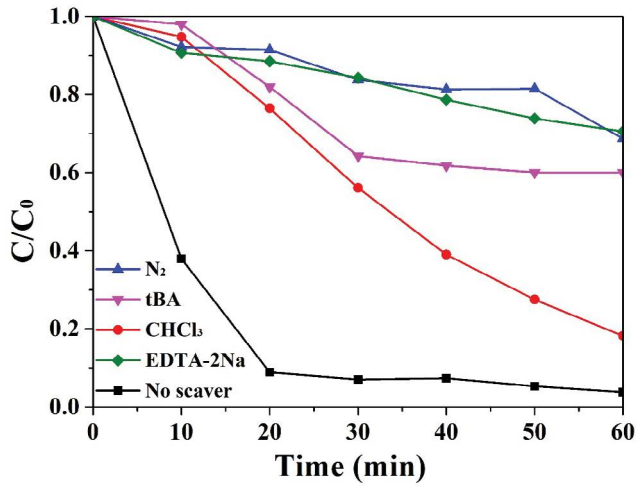

Fig. 7. Trapping experiments of active species during the photocatalytic ozonation degradation of 2,4-D over 0.5%-CoP/CN photocatalyst under visible light irradiation.

3.7. Photocatalytic mechanism

Based on the analysis mentioned above, a possible photocatalytic ozonation mechanism of CoP/g-C_3N_4 for 2,4-D degradation is proposed and shown in Fig. 8. Under visible-light irradiation, g-C_3N_4 is excited, and the photogenerated electrons and holes are produced on the conduction band (CB) and valence band. Due to the presence of CoP co-catalyst, electrons in CB can be easily transferred to CB of CoP, which can enhance the efficiency of charge separation of the g-C_3N_4 catalyst and improve the photocatalytic ozonation activity. Furthermore, CoP is also excited to separate photogenerated electron-hole pairs. The electrons can accumulate on the surface of CoP and can be trapped by the O_3 molecules and generate $^{\bullet}O_3^-$. Moreover, the as-generate $^{\bullet}O_3^-$ can react with H^+ in the solution to produce $^{\bullet}HO_3^-$ radicals for the formation of $^{\bullet}OH$. Therefore, ozone is an efficient scavenger for the photoinduced electrons, which could significantly promote the charge separation efficiency. On the other hand, the holes left on the CB can also directly react with 2,4-D to degrade pollutants. Finally, it can be concluded that the 2,4-D molecules can be degraded both by the generated h^+ and $^{\bullet}OH$ radicals.

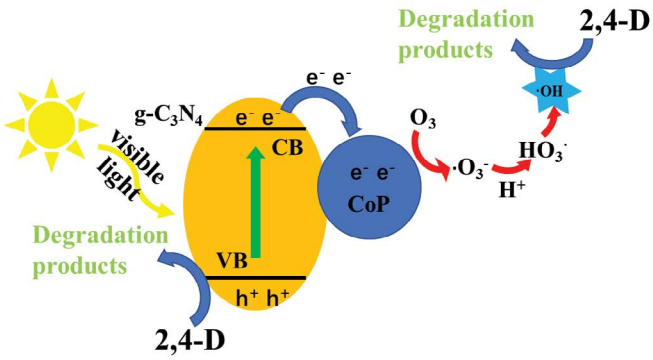

Fig. 8. Proposed mechanism of photocatalytic ozonation of 2,4-D for CoP/g-C_3N_4.

4. Conclusion

In the present work, CoP/g-C_3N_4 composite catalysts were successfully prepared through a solid-state-synthesis method. The as-prepared composites exhibited efficient photocatalytic ozonation performance for the degradation of 2,4-D (96.4%). The obvious improvement of CoP/g-C_3N_4 is mainly attributed to efficient separation of the electron-hole pairs resulting from the presence of the CoP cocatalyst, and the synergistic effects between ozonation and photocatalysis attributed to the powerful scavenger effect of ozone and strong activity of $^{\bullet}OH$ radicals.

Acknowledgments

This work is supported by the National Natural Science Foundation of China (21906039, 21906072), Natural Science Foundation of Shaanxi Province (2019JQ-382), Funding project for introduced overseas scholars of Hebei Province (C20190321), Fundamental Research Funds for the Central Universities of Chang'an University (300102290501), Program for water resources research and promotion of Hebei Province (2019–55), Doctoral research fund of Hebei Geo University (BQ2019041).

References

[1] F. Islam, J. Wang, M.A. Farooq, M.S. Khan, L. Xu, J. Zhu, M. Zhao, S. Muños, Q. Li, W. Zhou, Potential impact of the herbicide 2,4-dichlorophenoxyacetic acid on human and ecosystems, Environ. Int., 111 (2018) 332–351.

[2] Y.H. Zhou, P.Y. Li, M.J. Chen, Z.H. Dong, C.Y. Lu, Groundwater quality for potable and irrigation uses and associated health risk in southern part of Gu'an County, North China Plain, Environ. Geochem. Health, 2020, https://doi.org/10.1007/s10653–020–00553-y.

[3] M. Golshan, B. Kakavandi, M. Ahmadi, M. Azizi, Photocatalytic activation of peroxymonosulfate by TiO_2 anchored on cupper ferrite (TiO_2@ $CuFe_2O_4$) into 2,4-D degradation: process feasibility, mechanism and pathway, J. Hazard. Mater., 359 (2018) 325–337.

[4] G.D. Okcua, H.E. Oktenb, A. Yalcuk, Heterogeneous photocatalytic degradation and mineralization of 2,4-dichlorophenoxy acetic acid (2,4-D): its performance, kinetics, and economic analysis, Desal. Water Treat., 137 (2019) 312–327.

[5] W.L. Shi, M.Y. Li, X.L. Huang, H.J. Ren, F. Guo, Y.B. Tang, C.Y. Lu, Construction of $CuBi_2O_4/Bi_2MoO_6$ *p-n* heterojunction with nanosheets-on-microrods structure for improved photocatalytic activity towards broad-spectrum antibiotics degradation, Chem. Eng. J., 394 (2020) 125009–125018.

[6] E. Asgari, A. Esrafili, A.J. Jafari, R.R. Kalantary, M. Farzadki, Synthesis of TiO_2/polyaniline photocatalytic nanocomposite and its effects on degradation of metronidazole in aqueous solutions under UV and visible light radiation, Desal. Water Treat., 161 (2019) 228–242.

[7] R. Mohammadi, B. Massoumi, F. Galandar, Polyaniline-TiO_2/graphene nanocomposite: an efficient catalyst for the removal of anionic dyes, Desal. Water Treat., 142 (2019) 321–330.

[8] L.P. Wang, T.T. Huang, G.P. Yang, C.Y. Lu, F.L. Dong, Y.L. Li, W.S. Guan, The precursor-guided hydrothermal synthesis of $CuBi_2O_4/WO_3$ heterostructure with enhanced photoactivity under simulated solar light irradiation and mechanism insight, J. Hazard. Mater., 381 (2020) 120956–120967.

[9] M. Pirsaheb, K. Karimi, B. Shahmoradi, M. Moradi, Y. Vasseghian, E.N. Dragoi, Photocatalyzed degradation of acid orange 7 dye under sunlight and ultraviolet irradiation using Ni-doped ZnO nanoparticles, Desal. Water Treat., 165 (2019) 321–332.

[10] F. Tavakoli, A. Badiei, M.S. Niasari, Efficient photodegradation of acid orange 7 by using ultrasound-assisted synthesis of ternary graphene nanocomposite based on TiO_2, Desal. Water Treat., 147 (2019) 334–342.
[11] A. Akyol, Toxicity assessment and degradation of benzoquinone by ZnO photocatalytic oxidation process, Desal. Water Treat., 137 (2019) 202–211.
[12] F. Guo, X.L. Huang, Z.H. Chen, H.J. Ren, M.Y. Li, L.Z. Chen, MoS_2 nanosheets anchored on porous $ZnSnO_3$ cubes as an efficient visiblelight-driven composite photocatalyst for the degradation of tetracycline and mechanism insight, J. Hazard. Mater., 390 (2020) 122158–122169.
[13] E. Basturk, M. Işık, M. Karatas, Removal of aniline (Methylene Blue) and azo (Reactive Red 198) dyes by photocatalysis via nano TiO_2, Desal. Water Treat., 143 (2019) 306–313.
[14] W.L. Shi, M.Y. Li, X.L. Huang, H.J. Ren, C. Yan, F. Guo, Facile synthesis of 2D/2D $Co_3(PO_4)_2$/g-C_3N_4 heterojunction for highly photocatalytic overall water splitting under visible light, Chem. Eng. J., 382 (2019) 122960–122968.
[15] J.F. Guo, P.T. Li, Z. Yang, A novel Z-scheme g-C_3N_4/$LaCoO_3$ heterojunction with enhanced photocatalytic activity in degradation of tetracycline hydrochloride, Catal. Commun., 122 (2019) 63–67.
[16] N. Tian, H. Huang, Y. Guo, Y. He, Y. Zhang, A g-C_3N_4/$Bi_2O_2CO_3$ composite with high visible-light-driven photocatalytic activity for rhodamine B degradation, Appl. Surf. Sci., 322 (2014) 249–254.
[17] Q. Liang, J. Jin, C.H. Liu, S. Xu, C. Yao, Z.Y. Li, A stable $BiPO_4$/g-C_3N_4 nanosheet composite with highly enhanced visible light photocatalytic activity, J. Mater. Sci.-Mater. Electron., 29 (2018) 2509–2516.
[18] F. Guo, M.Y. Li, H.J. Ren, X.L. Huang, K.K. Shu, W.L. Shi, C.Y. Lu, Facile bottom-up preparation of Cl-doped porous g-C_3N_4 nanosheets for enhanced photocatalytic degradation of tetracycline under visible light, Sep. Purif. Technol., 228 (2019) 115770–115776.
[19] T. Tong, B. Zhu, C. Jiang, B. Cheng, J. Yu, Mechanistic insight into the enhanced photocatalytic activity of single-atom Pt, Pd or Au-embedded g-C_3N_4, Appl. Surf. Sci., 433 (2018) 1175–1183.
[20] K.Z. Qi, S.Y. Liu, R. Selvaraj, W. Wang, Z.X. Yan, Comparison of Pt and Ag as co-catalyst on g-C_3N_4 for improving photocatalytic activity: experimental and DFT studies, Desal. Water Treat., 153 (2019) 244–252.
[21] Y. Li, S. Wu, L. Huang, H. Xu, R. Zhang, M. Qu, Q. Gao, H. Li, g-C_3N_4 modified Bi_2O_3 composites with enhanced visible-light photocatalytic activity, J. Phys. Chem. Solids, 76 (2015) 112–119.
[22] T. Xiao, Z. Tang, Y. Yang, L. Tang, Y. Zhou, Z. Zou, In situ construction of hierarchical WO_3/g-C_3N_4 composite hollow microspheres as a Z-scheme photocatalyst for the degradation of antibiotics, Appl. Catal., B, 220 (2018) 417–428.
[23] K.Z. Qi, Y.B. Xie, R.D. Wang, S.Y. Liu, Z. Zhao, Electroless plating Ni-P cocatalyst decorated g-C_3N_4 with enhanced photocatalytic water splitting for H_2 generation, Appl. Surf. Sci., 466 (2019) 847–853.
[24] K.Z. Qi, W.X. Lv, I. Khan, S.Y. Liu, Photocatalytic H_2 generation via CoP quantum-dot-modified g-C_3N_4 synthesized by electroless plating, Chin. J. Catal., 41 (2020) 114–121.
[25] K.Z. Qi, Y. Li, Y.B. Xie, S.Y. Liu, K. Zheng, Z. Chen, R.D. Wang, Ag loading enhanced photocatalytic activity of g-C_3N_4 porous nanosheets for decomposition of organic pollutants, Front. Chem., 7 (2019) 91.
[26] J. Wang, P. Wang, C. Wang, Y. Ao, In-situ synthesis of well dispersed CoP nanoparticles modified CdS nanorods composite with boosted performance for photocatalytic hydrogen evolution, Int. J. Hydrogen Energy, 43 (2018) 14934–14943.
[27] X.J. Wang, X. Tian, Y.J. Sun, J.Y. Zhu, F.T. Li, H.Y. Mu, J. Zhao, Enhanced Schottky effect of a 2D-2D CoP/g-C_3N_4 interface for boosting photocatalytic H_2 evolution, Nanoscale, 10 (2018) 12315–12321.
[28] B. Luo, R. Song, J. Geng, X. Liu, D. Jing, M. Wang, C. Cheng, Towards the prominent cocatalytic effect of ultra-small CoP particles anchored on g-C_3N_4 nanosheets for visible light driven photocatalytic H_2 production, Appl. Catal., B, 256 (2019) 117819–117828.
[29] H. Li, J. Zhao, Y. Geng, Z. Li, Y. Li, J. Wang, Construction of CoP/B doped g-C_3N_4 nanodots/g-C_3N_4 nanosheets ternary catalysts for enhanced photocatalytic hydrogen production performance, Appl. Surf. Sci., 496 (2019) 143738–143746.
[30] M. Jourshabani, Z. Shariatinia, A. Badiei, Synthesis and characterization of novel Sm_2O_3/S-doped g-C_3N_4 nanocomposites with enhanced photocatalytic activities under visible light irradiation, Appl. Surf. Sci., 427 (2018) 375–387.
[31] J.H. Zhang, Y.J. Hou, S.J. Wang, X. Zhu, C.Y. Zhu, Z. Wang, C.J. Li, J.J. Jiang, H.P. Wang, M. Pan, C.Y. Su, A facile method for scalable synthesis of ultrathin g-C_3N_4 nanosheets for efficient hydrogen production, J. Mater. Chem. A, 6 (2018) 18252–18257.
[32] L.M. Cao, Y.W. Hu, S.F. Tang, A. Iljin, J.W. Wang, Z.M. Zhang, T.B. Lu, Fe-CoP electrocatalyst derived from a bimetallic prussian blue analogue for large-current-density oxygen evolution and overall water splitting, Adv. Sci., 5 (2018) 1800949–1800957.
[33] X. Yan, G.R. Wang, Y.P. Zhang, Q.J. Guo, Z.L. Jin, 3D layered nano-flower MoSx anchored with CoP nanoparticles form double proton adsorption site for enhanced photocatalytic hydrogen evolution under visible light driven, Int. J. Hydrogen Energy, 45 (2020) 2578–2592.
[34] C.Y. Lu, F. Guo, Q.Z. Yan, Z.J. Zhang, D. Li, L.P. Wang, Y.H. Zhou, Hydrothermal synthesis of type II $ZnIn_2S_4$/$BiPO_4$ heterojunction photocatalyst with dandelion-like microflower structure for enhanced photocatalytic activity under simulated solar light degradation of tetracycline, J. Alloys Compd., 811 (2019) 151976.
[35] J.L. Li, W.S. Guan, X. Yan, Z. Wu, W.D. Shi, Photocatalytic ozonation of 2,4-dichlorophenoxyacetic acid using $LaFeO_3$ photocatalyst under visible light irradiation, Catal. Lett., 148 (2018) 23–29.
[36] F. Guo, M.Y. Li, H.J. Ren, X.L. Huang, W.X. Hou, C. Wang, W.L. Shi, C.Y. Lu, Fabrication of *p-n* $CuBi_2O_4$/MoS_2 heterojunction with nanosheets-onmicrorods structure for enhanced photocatalytic activity towards tetracycline degradation, Appl. Surf. Sci., 491 (2019) 88–94.

Supplementary information

Table S1
Comparison of CoP/CN photocatalytic ozonation performance with other previously reported photocatalytic ozonation photocatalysts

Compounds	$C_{Compounds}$ (mg L^{-1})	Catalyst (g L^{-1})	$C_{catalyst}$ (g L^{-1})	O_3 concentration	DR %	TOC removal %	References
2,4-D	20	CoP/CN	0.8	14.2 mg/L 30 mL/min	96.4 (60 min)	88.2 (60 min)	This work
2,4-D	10	$LaFeO_3$	1.0	14.2 mg/L 60 mL/min	97 (60 min)	53 (60 min)	[S1]
Textile wastewater	10	Dy_2O_3/TiO_2/graphite/Ti	–	3 L/min	90 (90 min)	–	[S2]
Cefixime	5	N-TiO_2/GO/Ti	–	72 mg/L	91 (240 min)	–	[S3]
Ciprofloxacin	10	ZnO/stone	3.0	4 L/min	96 (30 min)	65% (5 h)	[S4]
Monuron	100	TiO_2/ceramic paper sheet	1.1	20 mg/L	Nearly 100 (50 min)	56 (50 min)	[S5]

References

[S1] J.L. Li, W.S. Guan, X. Yan, Z.Y. Wu, W.D. Shi, Photocatalytic ozonation of 2,4-dichlorophenoxyacetic acid using $LaFeO_3$ photocatalyst under visible light irradiation, Catal. Lett., 148 (2018) 23–29.

[S2] M. Sheydaei, D. Soleimani, B. Ayoubi-Feiz, Simultaneous immobilization of Dy_2O_3, graphite and TiO_2 to prepare stable nanocomposite for visible light assisted photocatalytic ozonation of a wastewater: modeling via artificial neural network, Environ. Technol. Innovation, 17 (2020) 100512.

[S3] M. Sheydaei, H.R.K. Shiadeh, B. Ayoubi-Feiz, R. Ezzati, Preparation of nano N-TiO_2/graphene oxide/titan grid sheets for visible light assisted photocatalytic ozonation of cefixime, Chem. Eng. J., 353 (2018) 138–146.

[S4] M. Malakootian, H. Mahdizadeh, A. Dehdarirad, M. Amiri Gharghani, Photocatalytic ozonation degradation of ciprofloxacin using ZnO nanoparticles immobilized on the surface of stones, J. Dispersion Sci. Technol., 40 (2019) 846–854.

[S5] G. Simon, T. Gyulavári, K. Hernádi, M. Molnár, Z. Pap, G. Veréb, K. Schrantz, M. Náfrádi, T. Alapi, Photocatalytic ozonation of monuron over suspended and immobilized TiO_2–study of transformation, J. Photochem. Photobiol., A, 356 (2018) 512–520.